Breakdown of the Sharvin limit in spin pumping with interfacial Rashba spin-orbit coupling

Ka Shen,[1,*] Lei Wang,[2] and Ke Xia[1,3,4]

[1]*Center for Advanced Quantum Studies and Department of Physics, Beijing Normal University, Beijing 100875, China*
[2]*Center for Spintronics and Quantum Systems, State Key Laboratory for Mechanical Behavior of Materials,*
Xi'an Jiaotong University, No. 28 Xianning West Road Xi'an, Shaanxi 710049, China
[3]*Shenzhen Institute for Quantum Science and Engineering, and Department of Physics,*
Southern University of Science and Technology, Shenzhen 518055, China
[4]*Center for Quantum Computing, Peng Cheng Laboratory, Shenzhen 518005, China*

We theoretically investigate the role of the interfacial Rashba spin-orbit coupling in spin pumping based on a nonperturbative calculation. A nonmonotonic behavior is predicted in the Rashba-strength dependence of the Gilbert damping coefficients. We show that the in-plane damping component can exceed the Sharvin limit thanks to the Rashba-field-induced torque. Nevertheless, the pumped spin current remains below the Sharvin limit and satisfies the Onsager reciprocity relations with the spin-current-induced spin-transfer torque.

I. INTRODUCTION

As a spin current in a nonmagnetic normal metal (NM) is reflected by or transmits through a ferromagnetic (FM) layer, the exchange of angular momentum between the spin current and the magnetic layer will rotate the polarization direction of the spin current and simultaneously exert a spin-transfer torque on the magnetization [1–4]. This phenomenon has been extensively studied in the past decades for its promising applications in future spintronic devices [5,6]. In a magneto-electronic dc circuit theory, the spin-transfer torque produced by the incoming spin current, due to spin accumulation $\boldsymbol{\mu}_s$, is expressed as [7]

$$\boldsymbol{\tau} \simeq g_r^{\uparrow\downarrow}\boldsymbol{m} \times \boldsymbol{\mu}_s \times \boldsymbol{m} + g_i^{\uparrow\downarrow}\boldsymbol{\mu}_s \times \boldsymbol{m}. \tag{1}$$

The first term is even with respect to the magnetization direction $\boldsymbol{m}$ and is usually referred to as the dampinglike torque, while the second one with linear order in $\boldsymbol{m}$ is a fieldlike torque. The parameters $g_r^{\uparrow\downarrow}$ and $g_i^{\uparrow\downarrow}$ are the real and imaginary parts of the phenomenological spin mixing conductance, which, in the literature, is usually written as [7–9]

$$g^{\uparrow\downarrow} = \sum_{nn'=1}^{N} \delta_{nn'} - r_{nn'}^{\uparrow}(r_{nn'}^{\downarrow})^*. \tag{2}$$

Here, $r_{nn'}^{\uparrow(\downarrow)}$ is the reflection coefficient of the spin-up (down) species from the n'th incoming channel of NM to the nth outgoing channel. Apparently, $g_r^{\uparrow\downarrow}$ from Eq. (2) has an upper limit of twice of the total transport channels, i.e., the Sharvin conductance [7]. This limit corresponds to the situation where all incoming electrons flip their transverse spin polarization.

The inverse process of the spin-current-induced torque is called spin pumping, where the magnetization dynamics of FM injects a spin current into a NM [8],

$$\boldsymbol{I}_s = g_r^{\uparrow\downarrow}\boldsymbol{m} \times \dot{\boldsymbol{m}} + g_i^{\uparrow\downarrow}\dot{\boldsymbol{m}}. \tag{3}$$

According to the angular momentum conservation, the torque acting back on the magnetization is

$$\boldsymbol{\tau} = -\boldsymbol{I}_s. \tag{4}$$

The first term in Eq. (3) is of the same structure as the Gilbert damping torque and gives rise to an enhancement of the Gilbert damping coefficient [8,10–15],

$$\Delta\alpha = \frac{\hbar\gamma}{4\pi M_s V} g_r^{\uparrow\downarrow}, \tag{5}$$

in which γ is the gyromagnetic ratio, M_s is the saturation magnetization, and V is the volume of the FM. Obviously, the damping enhancement given by Eq. (5) is also limited by the Sharvin conductance.

It is important to notice that Eqs. (1) and (3) are in principle valid only for an ideal situation without any other source of spin torques. However, at the interface of a NM | FM hybrid structure, an interfacial Rashba-type spin orbit coupling (SOC) does naturally exist and is able to supply spin-orbit torques [16–25]. This implies the incompleteness of Eqs. (1) and (3) and the possible breakdown of Eq. (4). One fundamental question one may ask is whether the interfacial SOC can break the Sharvin limit of the spin mixing conductance and/or the Gilbert damping enhancement discussed above. A perturbation approach was recently developed to study the effect of the interfacial Rashba SOC in spin pumping [19], where an interfacial spin memory loss [18,26] and an anisotropic correction to the Gilbert damping were shown. The SOC-induced anisotropic damping was recently observed in experiment [27]. The influence of SOC on the Sharvin limit motivates the present work.

As the perturbation approach is applicable only for weak SOCs, a general formalism for the Gilbert damping has been derived from the energy loss of the magnetic subsystem and written in the form of the scattering matrix $\hat{S}$ as [28,29]

$$\Delta\alpha_{ij} = \frac{\hbar\gamma}{4\pi M_s V}\text{Tr}\big(\partial_{m_i}\hat{S}\partial_{m_j}\hat{S}^\dagger\big). \tag{6}$$

*kashen@bnu.edu.cn

In this work, we employ this formalism to calculate the damping enhancement of ferromagnetic insulators (FMIs) in spin pumping by taking into account the Rashba SOC at the interface. We predict a nonmonotonic behavior in its dependence on the SOC strength with a peak forming in the intermediate SOC strength regime. The damping coefficient near the peak can become larger than the Sharvin limit. We find that these features are dominated by a few hot transport channels in momentum space and, according to an alternative two-potential-model calculation, result from the interference of the multiple reflection waves between the Rashba barrier and the interface potential. During such a multiple reflection process, a spin-orbit torque is gradually accumulated and transferred to FMIs mediated by the propagating electrons. In contrast, we find that the spin current injected into the NM remains below the Sharvin limit. We also calculate the spin-transfer torque induced by an incoming spin current and confirm the Onsager reciprocity relations.

II. MODEL

For an interface lying in the x-y plane, the total Hamiltonian reads

$$H(z) = \frac{\hat{\boldsymbol{p}}^2}{2m} + (V_0 + E_Z \boldsymbol{\sigma} \cdot \boldsymbol{m})\Theta(z)$$
$$+ \beta\delta(z - z_0)(\hat{p}_x \sigma_y - \hat{p}_y \sigma_x), \quad (7)$$

with E_Z and V_0 being the exchange energy and spin-independent potential in FMI ($z > 0$), respectively. The Rashba term locates at the interface ($z_0 = 0$). By solving the boundary conditions of the wave function

$$\Psi|_{0^+} = \Psi|_{0^-}, \quad (8)$$

$$\partial_z \Psi|_{0^-} - \partial_z \Psi|_{0^+} - 2m\beta(\hat{p}_x \sigma_y - \hat{p}_y \sigma_x)\Psi|_0 = 0, \quad (9)$$

under the interfacial potential, one can derive the scattering matrix. In the presence of the magnetization, it is convenient to solve Eqs. (8) and (9) under the spin basis with respect to the magnetization direction $\boldsymbol{m} = (\sin\theta\cos\phi, \sin\theta\sin\phi, \cos\theta)$, i.e.,

$$\chi^+ = \begin{pmatrix} e^{-i\phi/2}\cos(\theta/2) \\ e^{i\phi/2}\sin(\theta/2) \end{pmatrix}, \quad (10)$$

$$\chi^- = \begin{pmatrix} -e^{-i\phi/2}\sin(\theta/2) \\ e^{i\phi/2}\cos(\theta/2) \end{pmatrix}. \quad (11)$$

By substituting the scattered wave functions

$$\Psi^+_{z<0} = \chi^+ e^{ik_z z} + r^{++}\chi^+ e^{-ik_z z} + r^{-+}\chi^- e^{-ik_z z}, \quad (12)$$

$$\Psi^+_{z>0} = t^{++}\chi^+ e^{-\tilde{p}_+ k_z z} + t^{-+}\chi^- e^{-\tilde{p}_- k_z z}, \quad (13)$$

and

$$\Psi^-_{z<0} = \chi^- e^{ik_z z} + r^{--}\chi^- e^{-ik_z z} + r^{+-}\chi^+ e^{-ik_z z}, \quad (14)$$

$$\Psi^-_{z>0} = t^{--}\chi^- e^{-\tilde{p}_- k_z z} + t^{+-}\chi^+ e^{-\tilde{p}_+ k_z z}, \quad (15)$$

into Eqs. (8) and (9), we obtain the scattering/reflection matrix

$$\begin{pmatrix} r^{++} & r^{+-} \\ r^{-+} & r^{--} \end{pmatrix} = -1 + \frac{2}{(1 + iQ_1)(1 + iQ_2) + |P_1|^2}$$
$$\times \begin{pmatrix} 1 + iQ_2 & -iP_1 \\ -iP_1^* & 1 + iQ_1 \end{pmatrix} \quad (16)$$

with

$$Q_1 = \tilde{p}_+ - \tilde{\beta}\tilde{k}_\parallel \sin\theta \sin(\phi - \varphi), \quad (17)$$

$$Q_2 = \tilde{p}_- + \tilde{\beta}\tilde{k}_\parallel \sin\theta \sin(\phi - \varphi), \quad (18)$$

$$P_1 = -\tilde{\beta}\tilde{k}_\parallel[\cos\theta \sin(\phi - \varphi) - i\cos(\phi - \varphi)]. \quad (19)$$

Here, φ is the azimuthal angle of the incoming wave vector $\boldsymbol{k} = (k_\parallel \cos\varphi, k_\parallel \sin\varphi, k_z)$. Notice that the wave functions in FMI are all evanescent. The dimensionless quantities are $\tilde{p}_\pm = \sqrt{\tilde{k}_V^2 \pm \tilde{k}_Z^2 - 1}$, $\tilde{k}_V^2 = 2mV_0/k_z^2$, $\tilde{k}_Z^2 = 2mE_Z/k_z^2$, $\tilde{k}_\parallel = \sqrt{k_x^2 + k_y^2}/k_z$, and $\tilde{\beta} = 2m\beta$. With a unitary transform, we rewrite the scattering matrix under the spin basis along the $\hat{z}$ direction as

$$\hat{S}_{\boldsymbol{k}} = \frac{1}{\mathcal{F}}[2 + i(\tilde{p}_+ + \tilde{p}_-) - i(\tilde{p}_+ - \tilde{p}_-)\boldsymbol{m} \cdot \boldsymbol{\sigma}$$
$$+ 2i\tilde{\beta}\tilde{k}_\parallel \boldsymbol{h} \cdot \boldsymbol{\sigma}] - 1, \quad (20)$$

with $\boldsymbol{h} = \hat{z} \times \hat{k}$ being the direction of the Rashba field for a given wave vector $\boldsymbol{k}$. The third and fourth terms in the brackets of Eq. (20) reflect the spin precession about the exchange field and Rashba field, respectively. The factor

$$\mathcal{F} = 1 - \frac{(\tilde{p}_+ + \tilde{p}_-)^2}{4} + \left[\frac{\tilde{p}_+ - \tilde{p}_-}{2}\boldsymbol{m} - \tilde{\beta}\tilde{k}_\parallel\boldsymbol{h}\right]^2$$
$$+ i(\tilde{p}_+ + \tilde{p}_-), \quad (21)$$

revealing the interplay between them. The derivative of $\hat{S}_{\boldsymbol{k}}$ in Eq. (6) contains an additional piece due to the $\boldsymbol{m}$ dependence of $\mathcal{F}$, that is,

$$\partial_{m_j}\hat{S}_{\boldsymbol{k}} = \frac{-i(\tilde{p}_+ - \tilde{p}_-)}{\mathcal{F}}\sigma_j - (\hat{S}_{\boldsymbol{k}} + 1)\frac{1}{\mathcal{F}}\partial_{m_j}\mathcal{F}$$
$$= \frac{(\tilde{p}_+ - \tilde{p}_-)}{\mathcal{F}}[-i\sigma_j + \tilde{\beta}\tilde{k}_\parallel h_j(\hat{S}_{\boldsymbol{k}} + 1)], \quad (22)$$

leading to

$$\Delta\alpha_{ij} = \sum_{\boldsymbol{k}} \frac{2(\tilde{p}_+ - \tilde{p}_-)^2}{|\mathcal{F}|^2}\left[\delta_{ij} + 2(\tilde{\beta}\tilde{k}_\parallel)^2 h_i h_j \frac{(\tilde{p}_+ + \tilde{p}_-)^2}{|\mathcal{F}|^2}\right]. \quad (23)$$

The prefactor $\hbar\gamma(4\pi M_s V)$ has been omitted here.

III. RESULTS

A. Gilbert damping with interfacial Rashba SOC

As the inverse spin Hall measurement in spin pumping experiments requires the magnetization to be parallel to the interface [13,30–33], in the following we restrict ourselves to the in-plane magnetization configuration and, without loss of
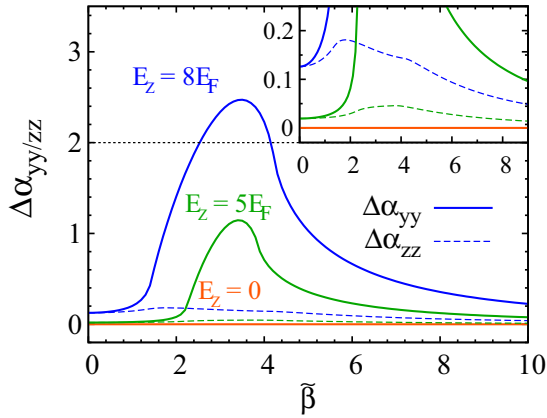
FIG. 1. Normalized enhanced damping component $\Delta\alpha_{yy}$ (solid curves) and $\Delta\alpha_{zz}$ (dashed curves) as functions of the Rashba coefficient with different exchange strengths. The black dotted curve represents the Sharvin limit. The inset zooms in the area with small values. In the calculation, we take $V_0 = 10E_F$ with $E_F = k_F^2/(2m)$ being the Fermi energy.

generality, take $\boldsymbol{m} \parallel \hat{x}$. Equation (23) thus gives two nonvanishing damping parameters:

$$\Delta\alpha_{yy} = \sum_k \frac{2(\tilde{p}_+ - \tilde{p}_-)^2}{|\mathcal{F}|^2}\left[1 + \frac{2\tilde{\beta}^2\tilde{k}_x^2(\tilde{p}_+ + \tilde{p}_-)^2}{|\mathcal{F}|^2}\right], \quad (24)$$

$$\Delta\alpha_{zz} = \sum_k 2(\tilde{p}_+ - \tilde{p}_-)^2/|\mathcal{F}|^2. \quad (25)$$

Obviously, both damping components vanish in the absence of the exchange coupling ($\tilde{p}_+ = \tilde{p}_-$). For a finite exchange strength, it is also easy to demonstrate that they reduce to the real part of Eq. (2), $g_r^{\uparrow\downarrow} = 2(\tilde{p}_+ - \tilde{p}_-)^2/[(1 - \tilde{p}_+\tilde{p}_-)^2 + (\tilde{p}_+ + \tilde{p}_-)^2]$, at a vanishing Rashba SOC.

The Rashba term modifies both damping components via the denominator

$$|\mathcal{F}|^2 = \left\{1 - \frac{(\tilde{p}_+ + \tilde{p}_-)^2}{4} + \left[\tilde{\beta}\tilde{k}_y + \frac{\tilde{p}_+ - \tilde{p}_-}{2}\right]^2 + \tilde{\beta}^2\tilde{k}_x^2\right\}^2 + (\tilde{p}_+ + \tilde{p}_-)^2 \quad (26)$$

and also introduces an additional piece in the in-plane damping coefficient. Although the correction in $|\mathcal{F}|^2$ can enhance both components, $\Delta\alpha_{zz}$ remains below the Sharvin limit for any parameters. Very interestingly, as shown in Fig. 1, the other component $\Delta\alpha_{yy}$ (normalized by the number of channels) is able to exceed the Sharvin limit "2"! This thus gives a positive answer to the question raised in the Introduction. In the rest of this paper, we will analyze the origin of this feature in detail.

In Fig. 1, both $\Delta\alpha_{yy}$ and $\Delta\alpha_{zz}$ behave nonmonotonically as the Rashba SOC strength increases. To understand this, we derive asymptotic expressions in weak and strong Rashba SOC limits.

In the weak Rashba SOC limit, we do Taylor expansion up to the leading (quadratic) order in the Rashba coefficient and obtain

$$\Delta\alpha_{yy} \simeq \frac{A}{6\pi}\frac{(p_+ - p_-)^2}{(p_+ p_-)^2}\left(3 + \frac{p_+^2 + p_-^2 + 4p_+ p_-}{p_+^2 p_-^2}\tilde{\beta}^2 k_F^2\right)k_F^4, \quad (27)$$

$$\Delta\alpha_{zz} \simeq \frac{A}{6\pi}\frac{(p_+ - p_-)^2}{(p_+ p_-)^2}\left(3 + 2\frac{\tilde{\beta}^2 k_F^2}{p_+ p_-}\right)k_F^4. \quad (28)$$

Both increase with Rashba strength [19]. Here, A represents the area of the cross section and k_F is the Fermi wave vector in the NM.

In the opposite limit, it is interesting to notice that $|\mathcal{F}|^2$ in Eq. (26) reaches a minimal value $(\tilde{p}_+ + \tilde{p}_-)^2$ once the wave vector satisfies the equation of circle,

$$k_x^2 + \left(k_y + \frac{p_+ - p_-}{2\tilde{\beta}}\right)^2 = k_r^2. \quad (29)$$

The radius reads

$$k_r = \frac{1}{\tilde{\beta}}\left[\frac{(p_+ + p_-)^2}{4} - k_z^2\right]^{1/2}, \quad (30)$$

inversely proportional to the Rashba strength. In the case of a large-gap FMI, $k_V^2 \pm k_Z^2 \gg k_F^2$, hence $k_r \simeq (\sqrt{k_V^2 + k_Z^2} + \sqrt{k_V^2 - k_Z^2})/(2\tilde{\beta})$, depending only on β, m, V_0, and E_Z. When the Rashba coefficient is as large as to have $k_r < k_F$, we estimate

$$\Delta\alpha_{yy} \simeq \frac{A(p_+ - p_-)^2}{2(p_+ + p_-)}\left(\frac{\sqrt{k_F^2 - k_r^2}}{\tilde{\beta}^2} + \frac{k_r^2}{\sqrt{k_F^2 - k_r^2}}\right), \quad (31)$$

$$\Delta\alpha_{zz} \simeq \frac{A(p_+ - p_-)^2}{2(p_+ + p_-)}\frac{\sqrt{k_F^2 - k_r^2}}{\tilde{\beta}^2}. \quad (32)$$

In particular, if $k_r \ll k_F$, we have $k_F^2 - k_r^2 \approx k_F^2$. As a result, both $\Delta\alpha_{yy}$ and $\Delta\alpha_{zz}$ become inversely proportional to $\tilde{\beta}^2$ and decrease with increasing Rashba strength. With the parameters used for Fig. 1, the second term in Eq. (31) is dominant, explaining the significant difference between $\Delta\alpha_{yy}$ and $\Delta\alpha_{zz}$.

In Fig. 2, we plot the contribution from different (lateral momentum) transport channels for three Rashba strengths. The circular shape defined in Eq. (29) is clearly seen. The upper panel ($\Delta\alpha_{yy}$) also shows hot spots with values much greater than 2, especially for those at the edge of the middle figure. This is because the additional term with $\tilde{k}_x^2$ in Eq. (24) diverges for $k_z \simeq k_F$. Physically, this means that the scattering channels with those wave vectors can dissipate spin angular momentum orders of magnitude more than simply flipping the spin of the incoming electrons. This, according to our discussion in the Introduction, implies a huge torque induced by the Rashba SOC.

We should point out that such features also exist when the magnetization tilts away from the x-y plane. In particular, for
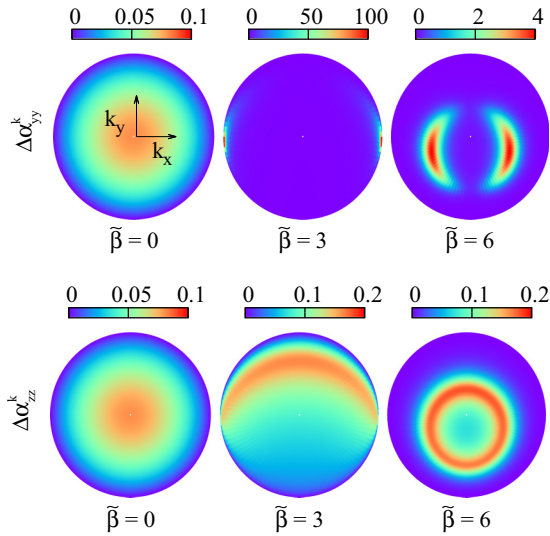
FIG. 2. Single channel contribution to Gilbert damping components in Eqs. (24) and (25) with in-plane magnetization $\boldsymbol{m}\|\hat{x}$. Here $V_0 = 10E_F$ and $E_Z = 8E_F$.

$\boldsymbol{m}\|\hat{z}$, at the circle in the momentum space

$$k_x^2 + k_y^2 = \frac{1}{\tilde{\beta}^2}(p_+p_- - k_z^2), \tag{33}$$

the factor

$$|\mathcal{F}|^2 = [1 - \tilde{p}_+\tilde{p}_- + (\tilde{\beta}\tilde{k}_\|)^2]^2 + (\tilde{p}_+ + \tilde{p}_-)^2 \tag{34}$$

arrives a minimum and gives rise to the huge enhancement. Note that the enhancement in this configuration is isotropic, i.e., $\Delta\alpha_{xx} = \Delta\alpha_{yy}$.

B. Two-potential model

To disclose the microscopic origin of such a huge SOC-induced torque, we slightly shift the Rashba SOC away from its natural location by introducing an infinitesimal $z_0 < 0$ in Eq. (7). The advantage of such a two-potential model is that, in addition to the total reflection matrix, it also supplies the detailed information of the interplay between the Rashba SOC and the exchange interaction. More specifically, it allows us to compute the spin torques acting on the magnetization and lattice (via the SOCs) from the net spin current within the inserting layer and the one injected into the NM, respectively.

The transmission and reflection matrices due to the Rashba SOC potential can be derived by using $-i$ to replace $\tilde{p}_\pm$ in Eqs. (13) and (15). The solutions are

$$\hat{t}_k = \frac{4 + 2i\tilde{\beta}\tilde{\boldsymbol{k}}_\| \times \boldsymbol{\sigma} \cdot \hat{z}}{4 + (\tilde{\beta}\tilde{k}_\|)^2}, \tag{35}$$

$$\hat{r}_k = \hat{t}_k - 1. \tag{36}$$

With the reflection matrix due to the potential barrier of FMI

$$\hat{r}_b = \hat{S}_{k\beta=0}, \tag{37}$$

it is straightforward to write out the overall reflection matrix by the two potentials

$$\hat{S}'_k = (1 + \hat{r}_b)(1 - \hat{r}_k\hat{r}_b)^{-1}\hat{t}_k - 1. \tag{38}$$
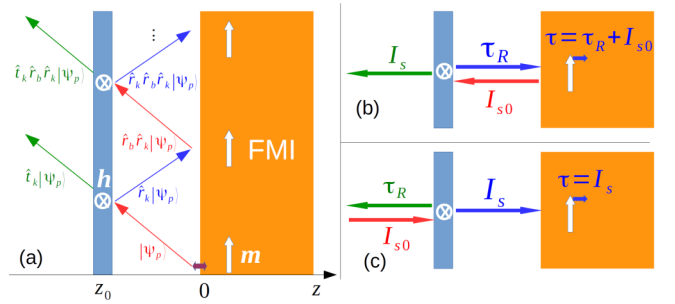
FIG. 3. (a) Scattering process in spin pumping configuration. Illustration of spin current flows and spin-transfer torques in (b) spin pumping and (c) spin-current-induced magnetization dynamics.

By substituting Eqs. (36) and (37), we get exactly the same result as $\hat{S}_k$ in Eq. (20) and reproduce Eqs. (24) and (25) by using Eq. (6).

On the other hand, in the spin pumping scenario of the present two-potential model, the variation of the magnetization direction in the FMI first creates a primary spin current into the inserting layer. Since there is no SOC at the modified NM | FMI interface, this pumped primary spin current is simply determined by Eq. (3). We describe the polarization of one individual electron contributing to this spin current by a set of wave functions leaving the FMI,

$$|\psi_p^{1\pm}\rangle = \sqrt{\tilde{g}_r^{\uparrow\downarrow}}|\pm\boldsymbol{m}\times\dot{\boldsymbol{m}}\rangle, \tag{39}$$

$$|\psi_p^{2\pm}\rangle = i\sqrt{|g_i^{\uparrow\downarrow}|}|\pm\dot{\boldsymbol{m}}\rangle, \tag{40}$$

with $|\pm\boldsymbol{\xi}\rangle$ representing the wave function with polarization along the $\pm\hat{\boldsymbol{\xi}}$ direction and amplitude $|\boldsymbol{\xi}|$. According to Eq. (16), the reflection coefficients at $z = 0$ are

$$r^\uparrow = r^{++} = \frac{1 - i\tilde{p}_+}{1 + i\tilde{p}_+}, \tag{41}$$

$$r^\downarrow = r^{--} = \frac{1 - i\tilde{p}_-}{1 + i\tilde{p}_-}, \tag{42}$$

and therefore the bare spin mixing conductance in Eqs. (39) and (40) can be expressed as

$$g_r^{\uparrow\downarrow} = \frac{2(\tilde{p}_+ - \tilde{p}_-)^2}{(1 - \tilde{p}_+\tilde{p}_-)^2 + (\tilde{p}_+ + \tilde{p}_-)^2}, \tag{43}$$

$$g_i^{\uparrow\downarrow} = -\frac{2(\tilde{p}_+ - \tilde{p}_-)(1 + \tilde{p}_+\tilde{p}_-)}{(1 - \tilde{p}_+\tilde{p}_-)^2 + (\tilde{p}_+ + \tilde{p}_-)^2}. \tag{44}$$

Further we write out the total left- and right-moving wave functions in the inserting layer after all orders of reflection process as

$$|\psi_l\rangle = |\psi_p\rangle + (1 - \hat{r}_b\hat{r}_k)^{-1}|\psi_p\rangle, \tag{45}$$

and

$$|\psi_r\rangle = \hat{r}_k(1 - \hat{r}_b\hat{r}_k)^{-1}|\psi_p\rangle, \tag{46}$$

respectively. The scattering processes are illustrated in Fig. 3(a). The total out-going wave function transmitted into

the NM reads

$$|\psi_T\rangle = \hat{t}_{\boldsymbol{k}}|\psi_l\rangle. \tag{47}$$

Note that, to imitate the realistic ($z_0 = 0$) situation, we have assumed that the inserting layer is too narrow to host a localized standing wave in between and we have disregarded the phase factor $e^{ik_z z}$ in the spatial wave function.

With the knowledge of the above wave functions, we compute the net spin current flowing within the inserting layer and the one going into the NM. The former gives the spin-transfer torque on the magnetization,

$$\boldsymbol{\tau}|_{\text{FMI}} = \langle\psi_r|\boldsymbol{\sigma}|\psi_r\rangle - \langle\psi_l|\boldsymbol{\sigma}|\psi_l\rangle, \tag{48}$$

and the latter reads

$$\boldsymbol{I}_s|_{\text{NM}} = \langle\psi_T|\boldsymbol{\sigma}|\psi_T\rangle. \tag{49}$$

In the calculation, we focus on the transport channels with the in-plane wave vector $\boldsymbol{k}\|\hat{x}$ because of the fact that the huge enhancement of Gilbert damping mainly comes from the finite-k_x channels [see Eq. (24) and Fig. 2]. Therefore, the Rashba field $\boldsymbol{h}\|\hat{y}$ is perpendicular to the exchange axis $\boldsymbol{m}$. By using $|\psi_p^{1\pm}\rangle$ and $|\psi_p^{2\pm}\rangle$ defined in Eqs. (39) and (40), we obtain

$$\boldsymbol{\tau}|_{\text{FMI}} = \left[\boldsymbol{\tau}(\psi_p^{1+}) - \boldsymbol{\tau}(\psi_p^{1-}) + \boldsymbol{\tau}(\psi_p^{2+}) - \boldsymbol{\tau}(\psi_p^{2-})\right]/2$$
$$= -\boldsymbol{m} \times \mathcal{G}_r \cdot \dot{\boldsymbol{m}} - \mathcal{G}_i \cdot \dot{\boldsymbol{m}} - G_{hh}\boldsymbol{h} \times \boldsymbol{h} \times \dot{\boldsymbol{m}}, \tag{50}$$

and

$$\boldsymbol{I}_s|_{\text{NM}} = \left[\boldsymbol{I}_s(\psi_p^{1+}) - \boldsymbol{I}_s(\psi_p^{1-}) + \boldsymbol{I}_s(\psi_p^{2+}) - \boldsymbol{I}_s(\psi_p^{2-})\right]/2$$
$$= G_r\boldsymbol{m} \times \dot{\boldsymbol{m}} + \mathcal{G}_i \cdot \dot{\boldsymbol{m}} - G_{hh}\boldsymbol{h} \times \boldsymbol{h} \times \dot{\boldsymbol{m}}$$
$$- 2G_h\boldsymbol{h} \times \dot{\boldsymbol{m}} + G_{hm}(\boldsymbol{h} \times \boldsymbol{m}) \times \dot{\boldsymbol{m}}, \tag{51}$$

where

$$\mathcal{G}_{rzz} = G_r, \tag{52}$$

$$\mathcal{G}_{ryy} = G_r\left(1 + \tilde{\beta}^2\tilde{k}_\|^2\right), \tag{53}$$

$$\mathcal{G}_{izz} = G_i, \tag{54}$$

$$\mathcal{G}_{iyy} = G_i - G_h\tilde{\beta}\tilde{k}_\|, \tag{55}$$

$$\mathcal{G}_{hh} = G_h\tilde{\beta}\tilde{k}_\|, \tag{56}$$

$$\mathcal{G}_{hm} = G_h(\tilde{p}_+ - \tilde{p}_-), \tag{57}$$

with $G_r = 2(\tilde{p}_+ - \tilde{p}_-)^2/|\mathcal{F}_{k_y=0}|^2$, $G_i = -2(\tilde{p}_+ - \tilde{p}_-)(1 + \tilde{p}_+\tilde{p}_-)/|\mathcal{F}_{k_y=0}|^2$, and $G_h = 2\tilde{\beta}\tilde{k}_\|(\tilde{p}_+ - \tilde{p}_-)/|\mathcal{F}_{k_y=0}|^2$.

Compared to the scalar parameters in Eq. (3), we now have two diagonal tensors, $\mathcal{G}_r$ and $\mathcal{G}_i$, in the first and second terms of Eq. (50). For the Gilbert damping tensor $\mathcal{G}_r$, the z component G_{rzz} is exactly the same as the expression in $\Delta\alpha_{zz}$ in Eq. (25). The y component G_{ryy} contains a correction proportional to $\tilde{\beta}^2\tilde{k}_\|^2$, which is very similar to $\Delta\alpha_{yy}$ in Eq. (24). As discussed in the previous section, this factor is the key of the huge damping. Notice that the prefactor in front of $\tilde{\beta}^2\tilde{k}_\|^2$ in Eq. (24) is missing in G_{ryy}, perhaps because of the fact that the higher-order effects due to the dynamics are not fully included in this simplified calculation. Nevertheless,

this simplified calculation does reproduce the main features of Eqs. (24) and (25).

Notice that for those hot spots in the upper middle plot in Fig. 2, the dimensionless lateral wave vector $\tilde{k}_\| \to \infty$, which leads to $\hat{t}_{\boldsymbol{k}} \sim 0$. In other words, the Rashba SOC confines these electrons within the inserting layer. During the continuously forth and back scatterings between the two scattering potentials, electrons receive the spin-orbit torque ($\boldsymbol{\tau}_R$) from the Rashba potential and release the torque to the interface with the FMI via the exchange interaction as illustrated in Fig. 3(b). As a consequence, the total spin torque acting on the magnetization is amplified by such a multiple-scattering process and the interference therein. We should point out that the interfacial "localized" states are actually not a crucial condition for a single channel to go beyond $G_{rzz} = 2$, as shown by the hot spots locating at the finite $\tilde{k}_\|$ regime in the upper right figure of Fig. 2.

Actually the dampinglike torque in Eq. (50) can be alternatively written as

$$\boldsymbol{m} \times \mathcal{G}_r \cdot \dot{\boldsymbol{m}} = G_r[\boldsymbol{m} \times \dot{\boldsymbol{m}} - \tilde{\beta}^2\tilde{k}_\|^2\boldsymbol{h} \times \boldsymbol{h} \times (\boldsymbol{m} \times \dot{\boldsymbol{m}})]. \tag{58}$$

The second piece in form of $\boldsymbol{h} \times \boldsymbol{h} \times (\boldsymbol{m} \times \dot{\boldsymbol{m}})$ however disappears in the pumped spin current in Eq. (51), indicating that the overdamped angular momentum in the FMI is compensated completely by the torque induced by the Rashba SOC. Since G_r is always smaller than 2, the pumped spin current cannot break the Sharvin limit as expected. The last two terms in Eq. (51) show that the presence of Rashba SOC also drives spin current components polarized along the magnetization direction.

Finally, we apply our two-potential model to test the Onsager reciprocal process of spin pumping, i.e., the magnetization dynamics driven by an spin current flowing toward the interface. For this purpose, we calculate the spin torque created by an incoming spin-polarized electronic wave function $|\psi_{\text{in}}\rangle$. After it transmits through the Rashba potential, similar to the spin pumping case discussed above, multiple scatterings happen. The overall wave functions of the left- and right-moving components in the inserting layer are now given by

$$|\psi_l\rangle = (1 - \hat{r}_{\boldsymbol{k}}\hat{r}_b)^{-1}\hat{t}_{\boldsymbol{k}}|\psi_{\text{in}}\rangle, \tag{59}$$

and

$$|\psi_r\rangle = \hat{r}_b|\psi_l\rangle. \tag{60}$$

We assume that the incoming spin current $\boldsymbol{I}_{s0}$ [see Fig. 3(c)] is driven by a spin chemical potential $\boldsymbol{\mu}_s$ and calculate the torque acting on the magnetization of FMI with the same technique discussed above. The incoming wave functions in these calculations are assumed to be

$$|\psi_{\text{in}}^\pm\rangle = |\pm\boldsymbol{\mu}_s\rangle. \tag{61}$$

The result can be expressed as

$$\boldsymbol{\tau} = [\boldsymbol{\tau}(\psi_{\text{in}}^+) - \boldsymbol{\tau}(\psi_{\text{in}}^-)]/2$$
$$= G_r\boldsymbol{m} \times \boldsymbol{\mu}_s \times \boldsymbol{m} + \mathcal{G}_i \cdot \boldsymbol{\mu}_s \times \boldsymbol{m} - 2G_h(\boldsymbol{h} \times \boldsymbol{\mu}_s) \times \boldsymbol{m}$$
$$+ G_{hh}(\boldsymbol{h} \times \boldsymbol{h} \times \boldsymbol{\mu}_s) \times \boldsymbol{m} - G_{hm}[(\boldsymbol{h} \times \boldsymbol{m}) \times \boldsymbol{\mu}_s] \times \boldsymbol{m}, \tag{62}$$

where the first two terms recover those in SOC-free magnetoelectronic dc circuit theory [see Eq. (1)], but with a correction due to the SOC. Actually, each piece in Eq. (62) can be obtained if we replace $\dot{\boldsymbol{m}}$ in Eq. (51) by $\boldsymbol{\mu}_s$ and add a global cross product $\times \boldsymbol{m}$. This suggests the Onsager reciprocal relations.

IV. SUMMARY

In summary, we have performed an analytical study on the spin pumping of the NM | FMI bilayer structure with the interfacial Rashba spin-orbit coupling fully included. The Gilbert damping shows a nonmonotonic behavior as the Rashba strength increases. Due to the additional torque generated by the Rashba spin-orbit coupling, the Gilbert damping coefficient can become larger than the upper limit given by a simple exchange model. This is consistent with a recent first-principles calculation [34]. Finally, we demonstrate that the interfacial Rashba interaction maintains the Onsager reciprocal relations between spin pumping and spin-transfer torque.

[1] J. Slonczewski, J. Magn. Magn. Mater. **159**, L1 (1996).

[2] L. Berger, Phys. Rev. B **54**, 9353 (1996).

[3] M. Tsoi, A. G. M. Jansen, J. Bass, W.-C. Chiang, M. Seck, V. Tsoi, and P. Wyder, Phys. Rev. Lett. **80**, 4281 (1998).

[4] E. B. Myers, D. C. Ralph, J. A. Katine, R. N. Louie, and R. A. Buhrman, Science **285**, 867 (1999).

[5] T. Kawahara, K. Ito, R. Takemura, and H. Ohno, Microelectron. Reliab. **52**, 613 (2012).

[6] K. L. Wang, J. G. Alzate, and P. K. Amiri, J. Phys. D: Appl. Phys. **46**, 074003 (2013).

[7] Y. Tserkovnyak, A. Brataas, G. E. W. Bauer, and B. I. Halperin, Rev. Mod. Phys. **77**, 1375 (2005).

[8] Y. Tserkovnyak, A. Brataas, and G. E. W. Bauer, Phys. Rev. Lett. **88**, 117601 (2002).

[9] Y. Tserkovnyak, A. Brataas, and G. E. W. Bauer, Phys. Rev. B **66**, 224403 (2002).

[10] S. Mizukami, Y. Ando, and T. Miyazaki, Jpn. J. Appl. Phys. **40**, 580 (2001).

[11] B. Heinrich, Y. Tserkovnyak, G. Woltersdorf, A. Brataas, R. Urban, and G. E. W. Bauer, Phys. Rev. Lett. **90**, 187601 (2003).

[12] B. Heinrich, C. Burrowes, E. Montoya, B. Kardasz, E. Girt, Y.-Y. Song, Y. Sun, and M. Wu, Phys. Rev. Lett. **107**, 066604 (2011).

[13] H. L. Wang, C. H. Du, Y. Pu, R. Adur, P. C. Hammel, and F. Y. Yang, Phys. Rev. Lett. **112**, 197201 (2014).

[14] Y. Yao, Q. Song, Y. Takamura, J. P. Cascales, W. Yuan, Y. Ma, Y. Yun, X. C. Xie, J. S. Moodera, and W. Han, Phys. Rev. B **97**, 224414 (2018).

[15] K.-R. Jeon, C. Ciccarelli, A. J. Ferguson, H. Kurebayashi, L. F. Cohen, X. Motiel, M. Eschrig, J. W. A. Robinson, and M. G. Blamire, Nat. Mater. **17**, 499 (2018).

[16] I. M. Miron, G. Gaudin, S. Auffret, B. Rodmacq, A. Schuhl, S. Pizzini, J. Vogel, and P. Gambardella, Nat. Mater. **9**, 230 (2010).

[17] K.-W. Kim, J.-H. Moon, K.-J. Lee, and H.-W. Lee, Phys. Rev. Lett. **108**, 217202 (2012).

[18] Y. Liu, Z. Yuan, R. J. H. Wesselink, A. A. Starikov, and P. J. Kelly, Phys. Rev. Lett. **113**, 207202 (2014).

[19] K. Chen and S. Zhang, Phys. Rev. Lett. **114**, 126602 (2015).

[20] V. P. Amin and M. D. Stiles, Phys. Rev. B **94**, 104419 (2016).

[21] V. P. Amin and M. D. Stiles, Phys. Rev. B **94**, 104420 (2016).

[22] L. Wang, R. J. H. Wesselink, Y. Liu, Z. Yuan, K. Xia, and P. J. Kelly, Phys. Rev. Lett. **116**, 196602 (2016).

[23] J. Borge and I. V. Tokatly, Phys. Rev. B **96**, 115445 (2017).

[24] V. P. Amin, J. Zemen, and M. D. Stiles, Phys. Rev. Lett. **121**, 136805 (2018).

[25] S. Li, K. Shen, and K. Xia, arXiv:1807.03433.

[26] J.-C. Rojas-Sánchez, N. Reyren, P. Laczkowski, W. Savero, J.-P. Attané, C. Deranlot, M. Jamet, J.-M. George, L. Vila, and H. Jaffrès, Phys. Rev. Lett. **112**, 106602 (2014).

[27] L. Chen, S. Mankovsky, S. Wimmer, M. A. W. Schoen, H. S. Korner, M. Kronseder, D. Schuh, D. Bougeard, H. Ebert, D. Weiss, and C. H. Back, Nat. Phys. **14**, 490 (2018).

[28] A. Brataas, Y. Tserkovnyak, and G. E. W. Bauer, Phys. Rev. Lett. **101**, 037207 (2008).

[29] A. Brataas, Y. Tserkovnyak, and G. E. W. Bauer, Phys. Rev. B **84**, 054416 (2011).

[30] E. Saitoh, M. Ueda, H. Miyajima, and G. Tatara, Appl. Phys. Lett. **88**, 182509 (2006).

[31] O. Mosendz, V. Vlaminck, J. E. Pearson, F. Y. Fradin, G. E. W. Bauer, S. D. Bader, and A. Hoffmann, Phys. Rev. B **82**, 214403 (2010).

[32] B. F. Miao, S. Y. Huang, D. Qu, and C. L. Chien, Phys. Rev. Lett. **111**, 066602 (2013).

[33] A. Azevedo, L. H. Vilela-Leão, R. L. Rodríguez-Suárez, A. F. Lacerda Santos, and S. M. Rezende, Phys. Rev. B **83**, 144402 (2011).

[34] L. Wang, Z. Yuan, K. Shen, G. E. W. Bauer, P. J. Kelly, and K. Xia (unpublished).